

PAPER

Nanostructural origin of semiconductivity and large magnetoresistance in epitaxial $\text{NiCo}_2\text{O}_4/\text{Al}_2\text{O}_3$ thin films

To cite this article: Congmian Zhen *et al* 2018 *J. Phys. D: Appl. Phys.* **51** 145308

View the [article online](#) for updates and enhancements.

Related content

- [Effect of interface on epitaxy and magnetism in h-RFeO₃/Fe₃O₄/Al₂O₃ films \(R = Lu, Yb\)](#)
Xiaozhe Zhang, Yuewei Yin, Sen Yang et al.
- [Topical Review](#)
Kathrin Dörr
- [From epitaxial growth of ferrite thin films to spin-polarized tunnelling](#)
Jean-Baptiste Moussy



IOP | ebooks™

Bringing you innovative digital publishing with leading voices to create your essential collection of books in STEM research.

Start exploring the collection - download the first chapter of every title for free.

Nanostructural origin of semiconductivity and large magnetoresistance in epitaxial $\text{NiCo}_2\text{O}_4/\text{Al}_2\text{O}_3$ thin films

Congmian Zhen^{1,2}, XiaoZhe Zhang^{2,3}, Wengang Wei^{1,4}, Wenzhe Guo¹, Ankit Pant², Xiaoshan Xu², Jian Shen⁴, Li Ma¹ and Denglu Hou¹

¹ Hebei Advanced Thin Films Laboratory, Department of Physics, Hebei Normal University, Shijiazhuang 050024, People's Republic of China

² Department of Physics and Astronomy, Nebraska Center for Materials and Nanoscience, University of Nebraska-Lincoln, NE 68588, United States of America

³ Department of Material Physics, School of Science, Xi'an Jiaotong University, Xi'an 710049, People's Republic of China

⁴ State Key Laboratory of Surface Physics and Department of Physics, Fudan University, Shanghai 200433, People's Republic of China

E-mail: xiaoshan.xu@unl.edu and cmzhen@hebtu.edu.cn

Received 15 January 2018, revised 13 February 2018

Accepted for publication 27 February 2018

Published 19 March 2018



CrossMark

Abstract

Despite low resistivity ($\sim 1 \text{ m}\Omega \text{ cm}$), metallic electrical transport has not been commonly observed in inverse spinel NiCo_2O_4 , except in certain epitaxial thin films. Previous studies have stressed the effect of valence mixing and the degree of spinel inversion on the electrical conduction of NiCo_2O_4 films. In this work, we studied the effect of nanostructural disorder by comparing the NiCo_2O_4 epitaxial films grown on MgAl_2O_4 (1 1 1) and on Al_2O_3 (0 0 1) substrates. Although the optimal growth conditions are similar for the NiCo_2O_4 (1 1 1)/ MgAl_2O_4 (1 1 1) and the NiCo_2O_4 (1 1 1)/ Al_2O_3 (0 0 1) films, they show metallic and semiconducting electrical transport, respectively. Post-growth annealing decreases the resistivity of NiCo_2O_4 (1 1 1)/ Al_2O_3 (0 0 1) films, but the annealed films are still semiconducting. While the semiconductivity and the large magnetoresistance in NiCo_2O_4 (1 1 1)/ Al_2O_3 (0 0 1) films cannot be accounted for in terms of non-optimal valence mixing and spinel inversion, the presence of anti-phase boundaries between nano-sized crystallites, generated by the structural mismatch between NiCo_2O_4 and Al_2O_3 , may explain all the experimental observations in this work. These results reveal nanostructural disorder as being another key factor for controlling the electrical transport of NiCo_2O_4 , with potentially large magnetoresistance for spintronics applications.

Keywords: nanostructural disorder, epitaxial film, NiCo_2O_4 , metallic electrical transport, semiconducting electrical transport

(Some figures may appear in colour only in the online journal)

1. Introduction

The recent discovery of metallicity in NiCo_2O_4 (NCO) has diversified the functional properties of the spinel material family in addition to their celebrated ferrimagnetism (e.g. in Fe_3O_4) [1–4]. The high conductivity and advantageous electrochemical properties of NCO are compelling for electrode

applications in energy storage devices such as metal-ion batteries and electrochemical supercapacitors [5–13]. On the other hand, the metallic conduction of NCO, i.e. low resistivity even at low temperatures, has only been observed in epitaxial thin films prepared in certain conditions [1–4], while in most cases insulating (or semiconducting) behavior has been reported [4, 14–21]. Therefore, many factors, including the

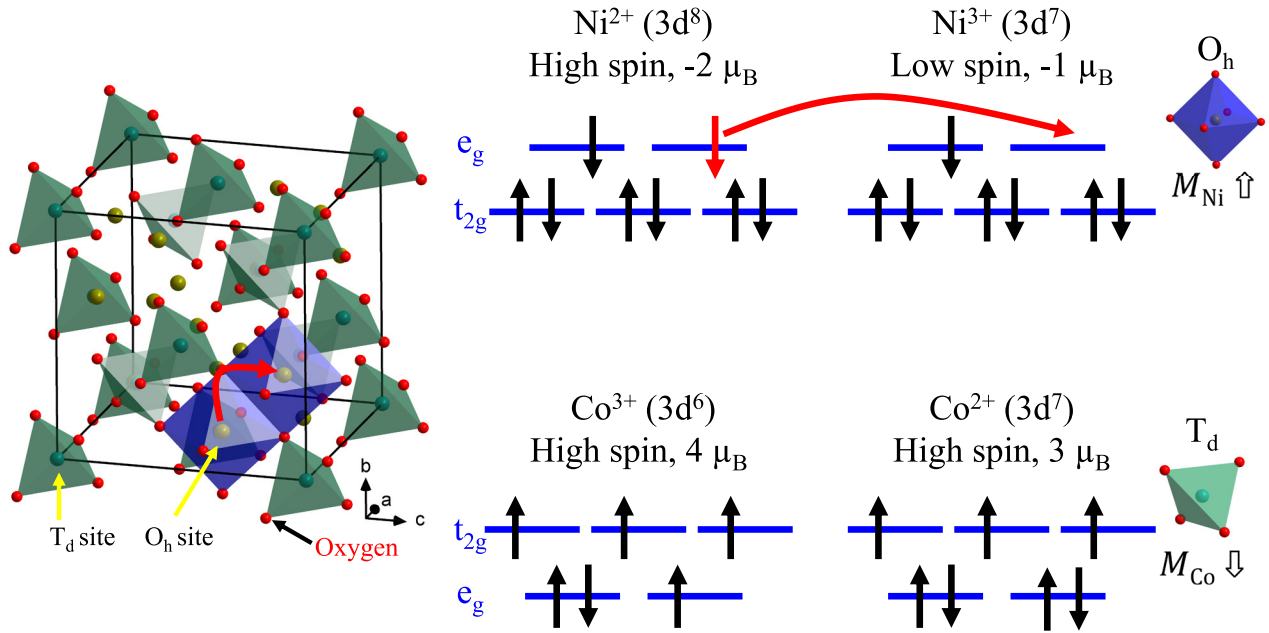


Figure 1. Left: the atomic model of the unit cell of NiCo_2O_4 in the inverse spinel crystal structure. The T_d sites are occupied by Co ions and the O_h sites are shared by Ni and Co ions. Only the local environments of two O_h sites are shown as shaded polyhedrons, while the local environments of all the T_d sites are shown. Right: the electronic configurations of Ni and Co ions on the O_h sites and T_d sites, respectively. The curved arrow indicates the nearest-neighbor hopping process.

crystal structure, nanostructure and electronic structure, are believed to be critical in the mechanism of electrical conduction in NCO.

NiCo_2O_4 has an inverse spinel crystal structure. In the unit cell, Co ions occupy sites with a tetrahedral (T_d) local environment, while Co ions and Ni ions share sites with an octahedral (O_h) local environment, as illustrated in figure 1 [2, 22]. The magnetic moments of the Ni and Co ions on the O_h and T_d sites respectively, are believed to be anti-aligned, corresponding to ferrimagnetic order below $T_C \approx 330\text{ K}$ [1, 2]. In contrast, the Co^{3+} ions on the O_h sites do not contribute to magnetization due to the zero-spin state ($e_g^0 t_{2g}^6$, $S = 0$) [22–25]. For the polycrystalline NCO, the measured resistivity always increases rapidly on cooling, corresponding to semiconducting behavior [15–21]. In contrast, high conductivity at low temperatures has been observed in epitaxial thin films grown on MgAl_2O_4 (MAO) and MgO substrates, indicative of metallicity [1–4]. The study of metallic and semiconducting NCO thin films, grown on MAO substrates under different conditions, suggests that the mixed valence of Ni^{2+} and Ni^{3+} on the O_h site and the double-exchange interactions are critical for the metallicity [2]. A comparison of the Raman spectroscopy of metallic and semiconducting NCO/MAO thin films demonstrates that the cation disorder on the O_h sites favors the metallicity [26]. Furthermore, the occupation of Ni on the O_h site instead of the T_d site was shown to be important for high conductivity in the textured NCO films grown on SrTiO_3 (STO) substrates [14].

In this work, we focus on the effect that the nanostructure of NCO films has on the conductivity. The transition between a metal and an insulating (or semiconducting) phase may be caused by changes to the electronic structure, such as band overlap and band filling changes; it may also be caused by

disorder, which localizes the electronic states [27, 28]. As shown in figure 1, the mixed valence (Ni^{2+} and Ni^{3+}) on the O_h sites allows the hopping of localized states (polarons), similar to that of Fe (Fe^{2+} and Fe^{3+}) on the O_h sites in Fe_3O_4 . As proposed previously, when the degree of valence mixing is high enough, the double-exchange interaction may make the e_g states on the Ni itinerant, generating metallic conduction [2]. Besides the degree of valence mixing, structural and nanostructural disorder may also be important in the localization of electrons. To investigate the effect of disorder on the nanostructure, we have studied the epitaxial NCO thin films grown on both MAO and Al_2O_3 (ALO) substrates. Due to the significant difference between the crystal structures of NCO and ALO, a structural anti-phase boundary is expected to exist and play a role in the conductivity. We found that although the optimal growth condition between the NCO (111)/ALO (001) and NCO (111)/MAO (111) films are similar, the NCO (111)/ALO (001) films show semiconducting behavior and the large dependence of resistivity on the film thickness. These results indicate the sensitivity of the electrical transport of NCO on the nanostructures, providing an insight into understanding the loss of metallicity in most polycrystalline samples.

2. Experimental section

Pulsed laser deposition (PLD) was employed to grow epitaxial NCO (111) thin films on $5\text{ mm} \times 5\text{ mm}$ ALO (001) and MAO (111) substrates, with various O_2 pressures (5–50 mTorr), growth temperatures (300 °C–500 °C), and thicknesses (24–95 nm) with a KrF excimer laser ($\lambda = 248\text{ nm}$, frequency = 10 Hz, fluence = 2.5 mJ cm^{-2}). The epitaxial relation between the film and substrate and the surface morphology of the films are monitored *in situ* by the reflection high

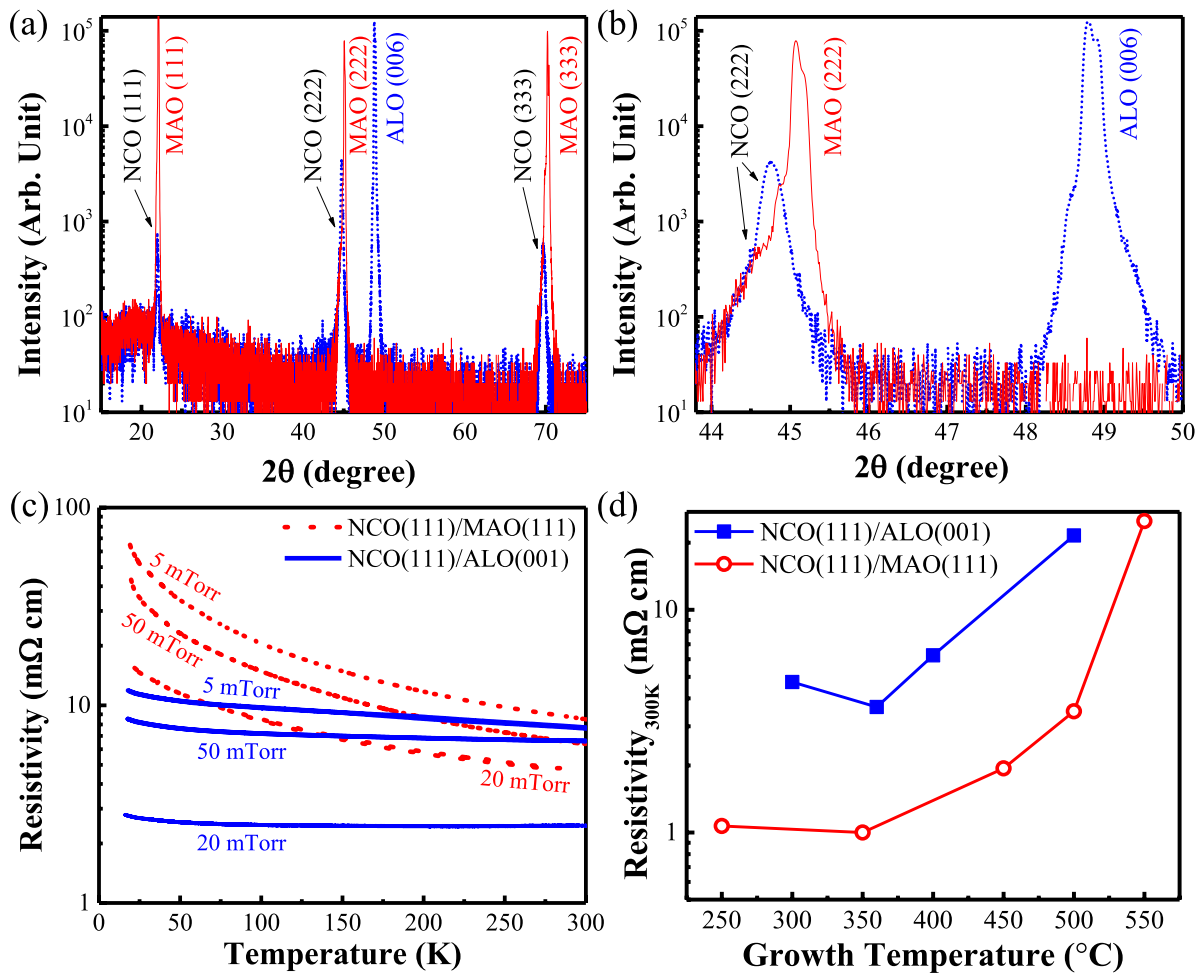


Figure 2. (a) $\theta/2\theta$ XRD spectra of NCO (111) films (95 nm) grown on MAO (111) and on ALO (001) substrates. (b) A close-up view of the spectra in (a) around the NCO (222) peak. (c) The temperature dependence of the resistivity of NCO (111) films at a different pressure on MAO (111) and on ALO (001) substrates. (d) Resistivity at 300 K of NCO (111) films grown on ALO (001) and MAO (111) substrates.

energy electron diffraction (RHEED). The crystallinity, thickness and out-of-plane lattice constants of the films were measured using x-ray diffraction (XRD) with a Rigaku D/Max-B x-ray diffractometer (Co K- α radiation, $\lambda = 1.789 \text{ \AA}$) and a Rigaku SmartLab x-ray diffractometer (copper K- α source, $\lambda = 1.54 \text{ \AA}$).

The surface morphology of the films was studied by atomic force microscopy. The electrical transport properties of the films were measured using the van der Pauw method. The magnetic properties of the films were examined using a superconducting quantum interference device (SQUID) magnetometer. A sequence of annealing on an NCO (111)/ALO (001) film of 96 nm was carried out using a tube furnace in one atm O_2 . For each annealing step, the film is heated for 3 h, followed by XRD at room temperature and transport measurements.

3. Results and discussion

3.1. Similar optimal growth conditions in NCO/MAO and NCO/ALO films

Previous studies have shown that both the growth temperature and the O_2 pressure are important factors for obtaining low

resistivity in NCO epitaxial thin films [1–4]. The consensus for the optimal growth temperature is about 350 °C [1–4, 14]. We have grown NCO films at various growth temperatures (300 °C–500 °C) and O_2 pressures (5–50 mTorr). The results indicate that the optimal growth temperature and O_2 pressure are about 360 °C and 20 mTorr respectively for both MAO and ALO substrates (figures 2(c) and (d)). As shown in figures 2(a) and (b), the XRD spectra indicate no impurity phase in the NCO films with the optimal growth conditions for both MAO and ALO substrates. While the NCO (111)/MAO (111) films show metallic behavior in optimal growth conditions (20 mTorr), all the NCO (111)/ALO (001) films show semiconducting behavior, even for optimal growth conditions (figure 2(c)).

3.2. Hopping conduction model and effect of cation disorder

For the NCO (111)/MAO (111) films (figure 3(a)), the resistivity does not change greatly in the range of thickness 24–95 nm. In stark contrast, for the NCO (111)/ALO (001) films, the resistivity increases rapidly when the film thickness decreases; the relative increase is larger at a lower temperature (figure 3(b)).

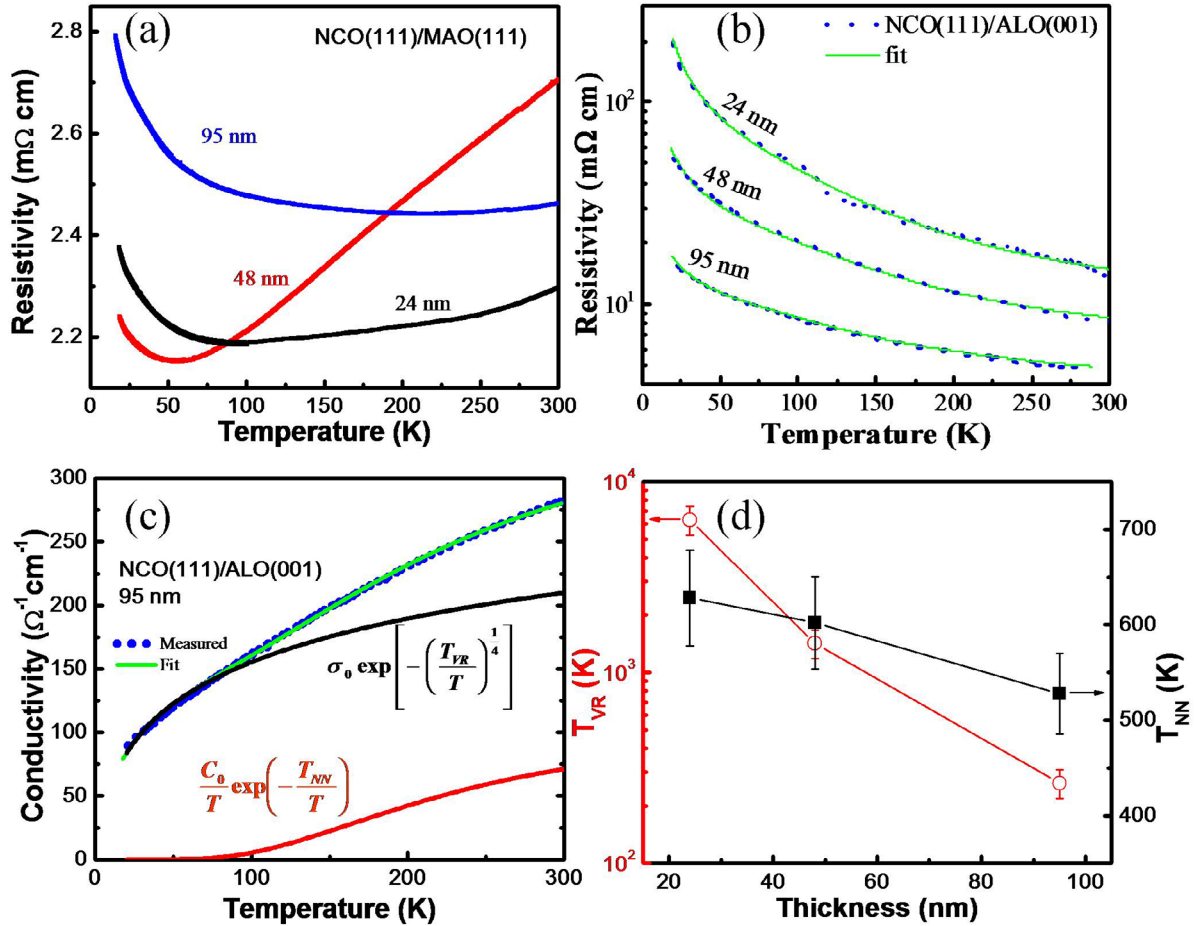


Figure 3. (a) The temperature dependence of NCO (111) films grown on MAO (111) of a different film thickness. (b) The temperature dependence of NCO (111) films grown on ALO (001) of different film thicknesses. The lines are fit using the hopping conduction model (see text). (c) The fit to the conductivity of the 95 nm film in (b) using the hopping conduction model. (d) Temperature parameters found in the fit in (b). All the films were grown in the optimal conditions.

In order to understand the mechanism of the electrical conduction in NCO (111)/ALO (001) films, we fit the temperature dependence of conductivity (σ) using the model of hopping conduction:

$$\sigma = \frac{1}{\rho} = \frac{C_0}{T} \exp\left(-\frac{T_{NN}}{T}\right) + \sigma_0 \exp\left[-\left(\frac{T_{VR}}{T}\right)^{\frac{1}{d+1}}\right]$$

where ρ is the resistivity, d is the dimension, T is temperature, and C_0 , σ_0 , T_{NN} and T_{VR} are the fitting parameters, of which the physical meaning will be discussed later. The first term describes the nearest-neighbor hopping and the second term describes the variable-range hopping. Previously, this model has been employed to explain the semiconducting behavior of NCO nanoplates ($d = 3$), in which the conductivity is in the range of that of the NCO (111)/ALO (001) films in figure 3(b) [16]. As shown in figure 3(b), all the curves can be fit using the hopping conduction model. The results of the fitting parameters T_{NN} and T_{VR} are plotted in figures 3(b) and (c). As shown in figure 3(c), the temperature dependence of the two effects is quite different. The nearest-neighbor hopping contributes more to the conductivity at a high temperature but diminishes quickly at low temperatures. In contrast, the variable range hopping contributes significantly at both high

and low temperatures, which is an indication of the important role played by disorder in the electrical transport. As shown in figure 3(c), T_{NN} changes slowly with the film thickness, while T_{VR} changes by more than one order of magnitude for the thickness range 24–95 nm.

In the model of hopping conduction, $k_B T_{NN}$ is the activation energy of the nearest-neighbor hopping, where k_B is the Boltzmann constant; the activation energy is found to be 54, 52 and 44 meV for the 24, 48 and 95 nm films, respectively. The previously reported nearest-neighbor hopping activation energy (66 meV) in nanoplates is also close to these values [16]. As depicted in figure 1, nearest-neighbor hopping is expected to occur between Ni ions on the O_h sites. In principle, the hopping of electrons from a Ni^{2+} ion to a Ni^{3+} ion on the O_h sites has the same initial and final electronic configuration ($Ni^{2+}Ni^{3+}$), i.e. the same initial and final energies. On the other hand, the Ni–O bond length changes according to the valence of the Ni ion. So, the hopping of electrons changes the local Ni–O distance, creating local structural distortion (phonons), which generates an energy barrier. Therefore, Ni^{2+} to Ni^{3+} hopping can be understood as a combination of electronic and vibrational excitations, or polarons. Polaron excitations have been observed in other mixed valent materials, such as Fe_3O_4 and $LuFe_2O_4$, with significantly larger hopping energies (about

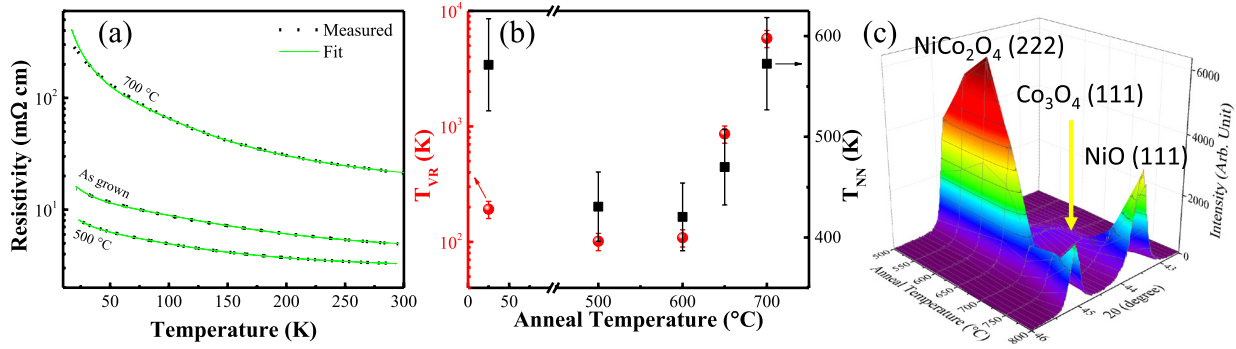


Figure 4. (a) The temperature dependence of resistivity of a 95 nm NCO (111)/ALO (001) film. (b) The hopping temperatures found by fitting the resistivity in (a) using the hopping conduction model. The values at 25 °C represent those found in the as-grown films. (c) The XRD around the NCO (222) peak after post-growth annealing at different temperatures.

0.16 and 0.25 eV, respectively) [29–31]. The relatively weak dependence of the activation energy on film thickness suggests that the local structure is only slightly affected by the film thickness. For variable-range hopping, $k_B T_{VR} = \frac{24}{\pi} \frac{1}{g\xi^d}$, where g is the density of state and ξ is the spatial extension (size) of the localized state. The dramatic change of T_{VR} suggests that the size of the localized states shrinks when the film is thinner.

Previous studies on NCO (001)/MAO (001) films show that the cation disorder is important for metallicity, which is believed to be an important reason for the low optimal growth temperature (≈ 350 °C) [14, 22, 26, 32]. In particular, the degree of spinel inversion, defined as the proportion of Ni ions on the O_h site, was also found to be critical for the high conductivity [14]. To investigate the effect of cation disorder on the conductivity of the NCO (111)/ALO (001) films, we studied their transport and structural properties after post-growth annealing. As shown in figure 4(a), after being annealed at 500 °C, the film shows substantially reduced resistivity. We fit the resistivity using the hopping conduction model, and the results are shown in figure 4(b). Both the nearest-neighbor hopping activation energy $k_B T_{NN}$ and the variable hopping temperature T_{VR} are reduced after annealing at 500 °C. This is consistent with the previous finding that annealing can increase the degree of spinel inversion and reduce the resistivity [14]. As shown in figures 4(a) and (b), further annealing at temperatures above 600 °C actually increases the resistivity, T_{NN} and T_{VR} again, the cause of which is revealed by the structural characterization. In figure 4(c), the $\theta/2\theta$ XRD spectra around the NCO (222) peak are displayed for different annealing temperatures. At above 600 °C, the peak intensity starts to decrease; eventually the NCO (111) peak splits into two, indicating the decomposition of NCO into NiO and Co_3O_4 . Although post-growth annealing below 600 °C decreases the resistivity of the NCO (111)/ALO (001) films substantially, the temperature dependence of the resistivity still shows semiconducting behavior. Therefore, the degree of spinel inversion is unlikely to cause the loss of metallicity in NCO (111)/ALO (001) films.

3.3. Effect of valence mixing

Previous studies on epitaxial thin films indicate that electronic structures, especially the valence mixing on Ni and Co, are

critical for metallicity in NCO. In the NCO (001)/MAO (001) films, the high growth temperature changes the degree of valence mixing and reduces the electrical conductivity, which is corroborated by the significant reduction of saturation magnetization [1, 2]. In the NCO (001)/MgO (001) films, the low O_2 growth environment affects the oxygen stoichiometry and reduces the electrical conductivity, which is accompanied by a large increase of saturation magnetization [3].

We measured the magnetic properties of the NCO (111)/MAO (111) and NCO (111)/ALO (001) films, because they have been demonstrated to be good indicators of electronic structures, especially valence mixing [1, 3]. As shown in figure 5(a), the temperature dependence of magnetization of the two films follow each other rather closely. The low-temperature field dependence of magnetization shows roughly a 10% difference in the saturation magnetization and slightly larger coercivity (figure 5(b)). The overall difference between the magnetic properties of the NCO (111)/MAO (111) and NCO (111)/ALO (001) films is modest, in comparison with the observation in the NCO (001)/STO (001) and NCO (001)/MgO (001) films [1, 3]. On the other hand, the magnetoresistance (MR) of the two films, defined as $[R(H) - R(0)]/R(H)$, shows dramatic differences (figure 5(c)), where R and H are the resistance and the magnetic field. While the NCO (111)/MAO (111) film has a small MR, in agreement with previous studies [1, 2], the NCO (111)/ALO (001) film exhibits a much larger MR at a low temperature. This temperature dependence and magnitude is consistent with that found in the Fe_3O_4 deposited on a MgO substrate [33, 34], which was interpreted as being the effect of the anti-phase boundary in the film [35, 36]. Therefore, it is unlikely that the absence of metallicity in NCO (111)/ALO (001) films is due to a significant change in the electronic structure, such as the valence mixing.

3.4. Effect of epitaxial strain

Next, we investigate the correlation between the structural properties of the NCO (111)/ALO (001) films and the resistivity. We start by looking at the epitaxial relations. Figures 6(a)–(d) show the diffraction pattern of the NCO (111)/ALO (001) film surface using RHEED. By comparing

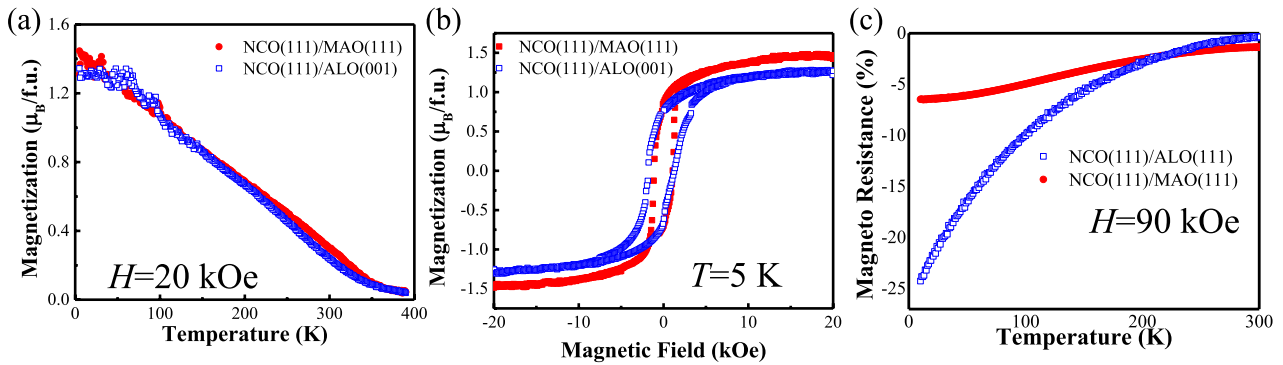


Figure 5. (a) The temperature dependence of the magnetization of NCO (111) films (95 nm) measured in a 20 kOe field on cooling. (b) The field dependence of magnetization of the NCO (111) films measured at 5 K. The films were grown in optimal conditions. (c) The magneto resistance defined as $[R(H) - R(0)]/R(H)$, as a function of temperature, where H is 90 kOe. The magnetic field is in the film plane. The films were grown in optimal conditions.

the diffraction pattern obtained when the electron beam is pointing in the same direction, one can obtain the in-plane epitaxial relation: ALO [120]/NCO [1 -10] and ALO [100]/NCO [11 -2]. The atomic arrangement of this epitaxial relation is illustrated using the models in figure 6(e). If we treat NCO [1 -10] and NCO [01 -1] as the basis of the NCO (111) plane 2D unit cell, the basis of the ALO (001) plane is rotated by 30° with respect to the basis of the NCO (111) plane. A similar epitaxial relation has been observed in the ALO (001)/ Fe_3O_4 (111) interface, which was explained in terms of the matching of the oxygen sublattice [37, 38].

One may estimate the possible epitaxial strain from figure 6(e) using the small mismatch of the oxygen sublattice in the ALO (001) plane and that of the NCO (111) plane; the result is a 4% in-plane compressive strain for the NCO (111) films. On the other hand, this strain appears to be mostly relaxed in the NCO (111)/ALO (001) films we have grown. As shown in figure 7(a), the d -spacing of the NCO (111) plane was measured using the $\theta/2\theta$ XRD, and the out-of-plane lattice constant was calculated for NCO films grown in various conditions. The out-of-plane lattice constant of the NCO (111) films grown on ALO (001) is only 0.4% larger than that of the bulk NCO, which is incompatible with the speculated 4% in-plane compressive strain. Therefore, the strain in the NCO (111)/ALO (001) films is mostly relaxed. In contrast, for the NCO (111)/MAO (111) films, the out-of-plane lattice constant is about 1% larger than that of bulk NCO, which agrees with that in the NCO (001)/MAO (001) films [1], indicating a small unrelaxed compressive strain up to at least 95 nm of film thickness. In addition, according to figure 7(a), the out-of-plane lattice constant of the NCO (111) film grown on ALO (001) does not appear to be sensitive to the growth temperature or the film thickness. Therefore, it is unlikely that the absence of metallicity of NCO (111)/ALO (001) films is due to the epitaxial strain.

3.5. Effect of nanostructural disorder

According to figure 6(e), the size of the in-plane unit cell of the NCO (111) plane and that of the ALO (001) plane do not have a one-to-one matching relation. This large difference in the size of the unit cells will generate structurally incompatible

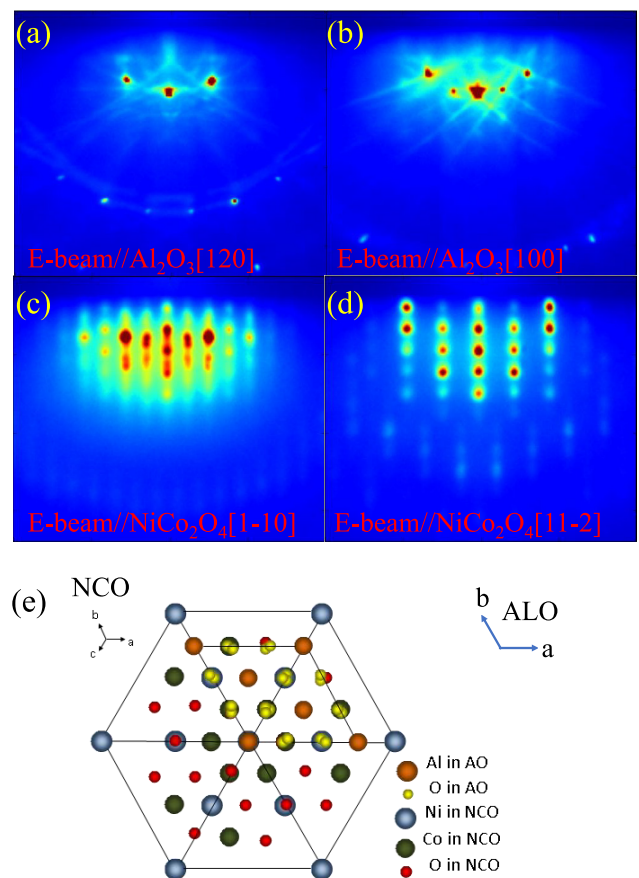


Figure 6. (a)–(d) The HEED images of different surfaces with two perpendicular directions of incident electron beam relative to the substrate. In (a) and (c), the orientation of the substrate is fixed so that the electron beam is parallel to ALO [120]. In (b) and (d), the orientation of the substrate is fixed so that the electron beam is parallel to ALO [100]. The alignment between the electron beams and the NCO film lattices is also indicated. (e) An atomic model of the epitaxial relation between NCO (111) and ALO (001) planes.

interfaces between crystallites nucleated at random positions. These interfaces, also called anti-phase boundaries, are expected to complicate the nanostructure, which was investigated here in the NCO (111)/ALO (001) films by the electron and XRDs. As shown in figures 6(c) and (d), the RHEED images of the NCO (111)/ALO (001) films show typical

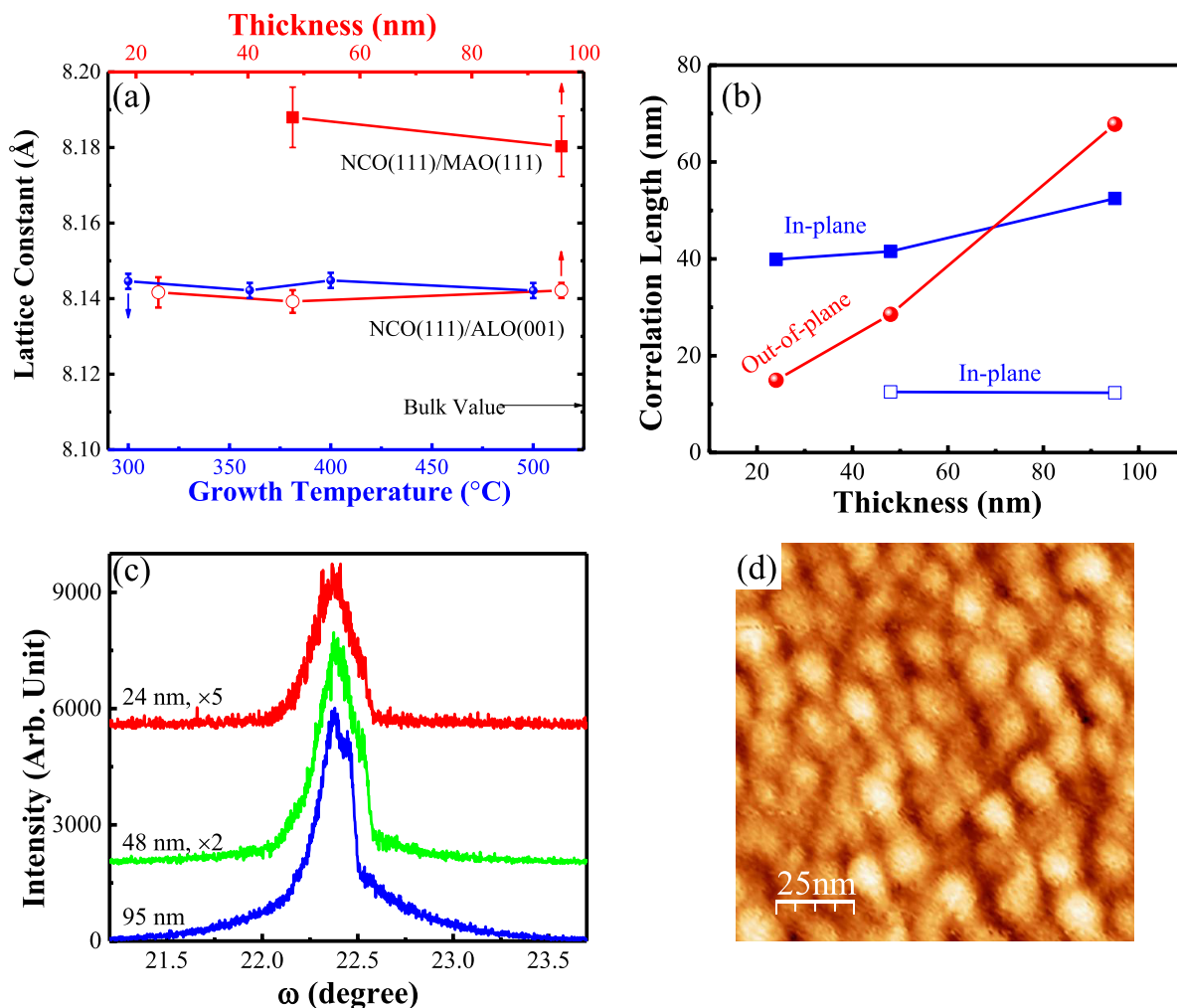


Figure 7. (a) The out-of-plane lattice constant of the NCO (1 1 1) films for different substrates and in different growth conditions. (b) The in-plane and out-of-plane structural correlation length of the NCO (1 1 1)/ALO (0 0 1) films as a function of film thickness. (c) The rocking curve of the NCO (1 1 1)/ALO (0 0 1) films of different film thickness. (d) An atomic force microscopy image of an NCO (1 1 1)/ALO (0 0 1) film (95 nm). The films in (b)–(d) were grown in optimal conditions.

patterns for quasi two-dimensional (2D) morphology, in that the vertical streaks and the arch-shaped arrangement indicate 2D reflection, while the array of diffraction spots indicates the formation of small islands. Further information on the nanostructure can be inferred from the structural correlation of the NCO films extracted from the XRDs. The out-of-plane structural correlation length can be estimated from the width of the $\theta/2\theta$ XRD peaks, and the result is shown in figure 7(b). As the film thickness increases, the structural correlation length also increases; the values are always smaller than the film thickness. The in-plane structural correlation length can be found from the XRD of the films (figure 7(c)): the rocking curve of the 48 nm and 95 nm NCO (1 1 1)/ALO (0 0 1) films shows a narrower peak standing on a broader peak, indicating two types of in-plane structural correlation length. While the longer in-plane correlation length (extracted from the narrower peak) increases with the film thickness, the shorter correlation length (extracted from the broader peak) remains relatively constant (about 12 nm) for the 48 and 95 nm films. The surface morphology of the NCO (1 1 1)/ALO (0 0 1) films was measured using atomic force microscopy (figure 7(d)).

Small crystallites of about 10 nm are observed at the film surface, which is consistent with the shorter structural correlation length found by the XRD. Hence, the structural correlation length—both in-plane and out-of-plane—increases with the film thickness.

The nanostructural disorder caused by anti-phase boundaries may account for all the above observations on the NCO (1 1 1)/ALO (0 0 1) films, as discussed below.

Under the same optimal growth conditions, the electronic structures and the cation distribution within every nano-sized crystallite of the NCO (1 1 1)/ALO (0 0 1) films is likely to be similar to those of the NCO (1 1 1)/MAO (1 1 1) films. Therefore, the magnitude and temperature dependence of the magnetization of the NCO (1 1 1)/ALO (0 0 1) films, which reflects their local properties, are expected to be similar to those of the NCO (1 1 1)/MAO (1 1 1) films; this agrees with the observation in figures 5(a) and (b). On the other hand, for the electrical conduction, the interfaces (anti-phase boundaries) between crystallites play extremely important roles. Due to these anti-phase boundaries, the electrons get localized and adopt the hopping mechanism for conduction; the spatial

extension of the localized states in the variable-range hopping is then related to the size of the crystallite. According to the analysis in figures 3(b) and (c), the T_{VR} decreases with the film thickness, indicating that the spatial extension of the localized states ξ increases with the film thickness; this is consistent with the observation (figure 7(b)) that the correlation length of the film, which is related to the size of the crystallites, increases with the film thickness.

Because the anti-phase boundaries originate from the structural mismatch between the film and the substrates, and because of the random location of the nucleation during the film growth, post-growth annealing is unlikely to remove the anti-phase boundaries. Therefore, the spatial extension of the localized states is not expected to change significantly during annealing; this is corroborated by the observation of the modest change of T_{VR} after annealing up to 600 °C. In contrast, the crystallinity within every crystallite can be improved by the annealing, as indicated by the obvious change of T_{NN} after annealing up to 600 °C, because high crystallinity is expected to reduce the nearest-neighbor hopping barrier.

The electrical conduction between crystallites may also depend on the relative spin alignment between the two sides of the interfaces. In other words, the crystallite/anti-phase boundary/crystallite may behave like a spin valve. Since the initial and final states of the hopping are similar at different sites, parallel spin alignment is favored for lower resistance. Thus, negative magnetoresistance is expected, which is consistent with the observation in figure 5(c). In this case, the greater interface causes larger magnetoresistance, which is why the magnetoresistance is much larger in the NCO (1 1 1)/ALO (00 1) films than in the NCO (1 1 1)/MAO (00 1) films.

4. Conclusions

To study the metallicity in NCO, we have compared the epitaxial NCO (1 1 1) films grown on MAO (1 1 1) and ALO (00 1) substrates. Despite the same optimal growth conditions, the NCO (1 1 1)/MAO (1 1 1) films are metallic, while the NCO (1 1 1)/ALO (00 1) films are semiconducting. The magnetic properties and the effect of post-growth annealing suggest that the known mechanism for the absence of metallicity in NCO, such as the deviation from the optimal valence mixing and the optimal cation occupancy, are not the origin of semiconductivity in NCO (1 1 1)/ALO (00 1) films. On the other hand, the presence of anti-phase boundaries, which originate from the mismatch between the crystal structures of NCO and ALO, as well as the random nucleation during the film growth, may explain all the observations in the NCO (1 1 1)/ALO (00 1) films, including the thickness dependence of the resistivity, the effect of post-growth annealing, the similarity between the magnetization of the NCO (1 1 1)/MAO (1 1 1) films and that of the NCO (1 1 1)/ALO (00 1) films, and the sign and large magnitude of the magnetoresistance in NCO (1 1 1)/ALO (00 1) films. Therefore, we propose that the nanostructural disorder caused by the anti-phase boundaries between the crystallites in the NCO (1 1 1)/ALO (00 1) films is the main factor for the absence of metallicity. These

findings shed important light on the absence of the metallic behavior of NCO in various forms, especially in polycrystalline samples. The large magnetoresistance in the NCO/ALO films can be exploited for potential spintronic applications.

Acknowledgments

This project was primarily supported by the National Science Foundation (NSF), DMR under award DMR-1454618 and by the Nebraska Center for Energy Sciences Research. C M Zhen would like to acknowledge the support provided by the Key Project of Natural Science of Hebei Higher Education under grant no. ZD2017045. The research was performed in part in the Nebraska Nanoscale Facility: National Nanotechnology Coordinated Infrastructure, and the Nebraska Center for Materials and Nanoscience, which are supported by the National Science Foundation under award ECCS: 1542182, and the Nebraska Research Initiative.

ORCID iDs

Congmian Zhen  <https://orcid.org/0000-0002-9652-3257>
Xiaoshan Xu  <https://orcid.org/0000-0002-4363-392X>

References

- [1] Silwal P, Miao L, Stern I, Zhou X, Hu J and Kim D H 2012 *Appl. Phys. Lett.* **100** 2012
- [2] Bitla Y et al 2015 *Sci. Rep.* **5** 15201
- [3] Li P, Xia C, Li J, Zhu Z, Wen Y, Zhang Q, Zhang J, Peng Y, Alshareef H N and Zhang X 2017 *ACS Nano* **11** 5011
- [4] Zhang K Q, Zhen C M, Wei W G, Guo W Z, Tang G D, Ma L, Hou D L and Wu X C 2017 *RSC Adv.* **7** 36026
- [5] Wu Z, Zhu Y and Ji X 2014 *J. Mater. Chem. A* **2** 14759
- [6] Dubal D P, Gomez-Romero P, Sankapal B R and Holze R 2015 *Nano Energy* **11** 377
- [7] Alcántara R, Jaraba M, Lavela P and Tirado J L 2002 *Chem. Mater.* **14** 2847
- [8] Zhang G Q, Bin Wu H, Hoster H E, Chan-Park M B and Lou X W 2012 *Energy Environ. Sci.* **5** 9453
- [9] Zhang G and Lou X W 2013 *Adv. Mater.* **25** 976
- [10] Li J, Xiong S, Liu Y, Ju Z and Qian Y 2013 *ACS Appl. Mater. Interfaces* **5** 981
- [11] Slater M D, Kim D, Lee E and Johnson C S 2013 *Adv. Funct. Mater.* **23** 947
- [12] Chen Y, Zhu J, Qu B, Lu B and Xu Z 2014 *Nano Energy* **3** 88
- [13] Li B, Feng J, Qian Y and Xiong S 2015 *J. Mater. Chem. A* **3** 10336
- [14] Ndione P F, Shi Y, Stevanovic V, Lany S, Zakutayev A, Parilla P A, Perkins J D, Berry J J, Ginley D S and Toney M F 2014 *Adv. Funct. Mater.* **24** 610
- [15] Windisch C F, Ferris K F and Exarhos G J 2001 *J. Vac. Sci. Technol. A* **19** 1647
- [16] Hu L, Wu L, Liao M, Hu X and Fang X 2012 *Adv. Funct. Mater.* **22** 998
- [17] Hu L, Wu L, Liao M and Fang X 2011 *Adv. Mater.* **23** 1988
- [18] Vemuri R S, Bharathi K K, Gullapalli S K and Ramana C V 2010 *ACS Appl. Mater. Interfaces* **2** 2623
- [19] Fujishiro Y, Hamamoto K, Shiono O, Katayama S and Awano M 2004 *J. Mater. Sci., Mater. Electron.* **15** 769
- [20] Windisch C F, Ferris K F, Exarhos G J and Sharma S K 2002 *Thin Solid Films* **420–1** 89

- [21] Windisch J, Exarhos G J, Ferris K F, Engelhard M H and Stewart D C 2001 *Thin Solid Films* **398–9** 45
- [22] Marco J F, Gancedo J R, Gracia M, Gautier J L, Ríos E I, Palmer H M, Greaves C and Berry F J 2001 *J. Mater. Chem.* **11** 3087
- [23] Dutta P, Seehra M S, Thota S and Kumar J 2008 *J. Phys.: Condens. Matter* **20** 15218
- [24] Mousavand T, Naka T, Sato K, Ohara S, Umetsu M, Takami S, Nakane T, Matsushita A and Adschiri T 2009 *Phys. Rev. B* **79** 144411
- [25] Lima A F 2015 *J. Phys. Chem. Solids* **91** 86
- [26] Iliev M N, Silwal P, Loukya B, Datta R, Kim D H, Todorov N D, Pachauri N and Gupta A 2013 *J. Appl. Phys.* **114** 033514
- [27] Imada M, Fujimori A and Tokura Y 1998 *Rev. Mod. Phys.* **70** 1039
- [28] Lee P A and Ramakrishnan T V 1985 *Rev. Mod. Phys.* **57** 287
- [29] Gasparov L V, Tanner D B, Romero D B, Berger H, Margaritondo G and Forró L 2000 *Phys. Rev. B* **62** 7939
- [30] Ikeda N et al 2005 *Nature* **43** 1136
- [31] Xu X S et al 2008 *Phys. Rev. Lett.* **101** 227602
- [32] Silwal P, La-O-Vorakiat C, Chia E E M, Kim D H and Talbayev D 2013 *AIP Adv.* **3** 092116
- [33] Venkateshvaran D, Althammer M, Nielsen A, Geprägs S, Rao M S R, Goennenwein S T B, Opel M and Gross R 2009 *Phys. Rev. B* **79** 134405
- [34] Eerenstein W, Palstra T T M, Saxena S S and Hibma T 2002 *Phys. Rev. Lett.* **88** 247204
- [35] McKenna K P, Hofer F, Gilks D, Lazarov V K, Chen C, Wang Z and Ikuhara Y 2014 *Nat. Commun.* **5** 5740
- [36] Margulies D T, Parker F T, Rudee M L, Spada F E, Chapman J N, Aitchison P R and Berkowitz A E 1997 *Phys. Rev. Lett.* **79** 5162
- [37] Zhang X, Yin Y, Yang S, Yang Z and Xu X 2017 *J. Phys.: Condens. Matter* **29** 164001
- [38] Zhang X, Yang S, Yang Z and Xu X 2016 *J. Appl. Phys.* **120** 85313